JOURNAL OF THE ROYAL SOCIETY Interface

Balancing on tightropes and slacklines

P. Paoletti and L. Mahadevan

J. R. Soc. Interface 2012 **9**, doi: 10.1098/rsif.2012.0077 first published online 18 April 2012

JOURNAL OF THE ROYAL SOCIETY Interface

J. R. Soc. Interface (2012) **9**, 2097–2108
doi:10.1098/rsif.2012.0077
Published online 18 April 2012

Balancing on tightropes and slacklines

P. Paoletti[1] and L. Mahadevan[1,2,3,*]

[1]*School of Engineering and Applied Sciences,* [2]*Department of Organismic and Evolutionary Biology, and* [3]*Wyss Institute for Bioinspired Engineering, Harvard University, Cambridge, MA 02138, USA*

Balancing on a tightrope or a slackline is an example of a neuromechanical task where the whole body both drives and responds to the dynamics of the external environment, often on multiple timescales. Motivated by a range of neurophysiological observations, here we formulate a minimal model for this system and use optimal control theory to design a strategy for maintaining an upright position. Our analysis of the open and closed-loop dynamics shows the existence of an optimal rope sag where balancing requires minimal effort, consistent with qualitative observations and suggestive of strategies for optimizing balancing performance while standing and walking. Our consideration of the effects of nonlinearities, potential parameter coupling and delays on the overall performance shows that although these factors change the results quantitatively, the existence of an optimal strategy persists.

Keywords: balance; tightrope; slackline

1. INTRODUCTION

Postural balance in humans requires active control because the normal upright position is mechanically unstable. Indeed, a stable upright stance can only be achieved by exploiting a feedback mechanism that creates a corrective torque based on multiple sensory inputs associated with body swaying [1]. In addition to its intrinsic neuromechanical importance, understanding the mechanisms involved with balance may help in the design of biped robots [2], in the diagnosis and amelioration of motor control problems in a range of neurological ailments [3,4], as well as in analysing games, such as stick-balancing [5] and even possibly in the active stabilization of large structures, such as buildings [6].

Most studies on postural balance are restricted to static or externally controlled platforms [7] where the active feedback between body motion and the dynamics of the environment is limited. Here, we consider the neuromechanical task of balancing on a soft dynamic support since this couples the internal dynamics of the body to the external dynamics induced by the body in a relatively simple setting, and thus begs the question of how the body can sense and then optimize its response to a dynamic environment. In addition, by considering the separate timescales associated with the response of the body and the controllable environment, we can begin to potentially probe the sensory-motor dynamics of the body as a function of age, size, health, etc.

A variety of models have been proposed to describe the dynamics of body sway motion during balancing on a fixed or moving platform [8,9]. Most of them reduce to the dynamics of a single degree-of-freedom system where the body is represented as an inverted pendulum; this simplification allows researchers to easily analyse the dynamics and control issues that arise for obtaining insight into postural balance strategies implemented by neural controllers [1,9–12]. An important aspect in all these studies requires the estimation of the body's current spatial orientation, which is clearly important to generate the necessary corrective action for stabilizing the mechanically unstable upright stance. In humans, this information about actual deviations from the upright position involves several proprioceptive, visual and vestibular sensory systems [13] and the relative importance of these mechanisms has led to a proposal of sensory channel reweighting accordingly to the strengths of different perturbative stimuli [7,13]. Thus, vestibular feedback sensors are thought to be more relevant on moving platforms, whereas proprioceptive and visual systems are the primary feedback sensors during quiet standing [13]. Furthermore, the presence of delay in the feedback loop has a non-negligible impact on the overall performance [8,14].

When balancing on a rope rather than on a rigid substrate, the neuromechanical dynamics of the body is coupled with the external dynamics of the rope which itself moves in response to body swaying. To address how balance might be achieved in this system, we need to understand the passive coupled dynamics of the system, sensory modalities that allow the body to infer its orientation and activate motor coordination to maintain or regain balance.

In §2, we present a minimal mechanical model for the body–rope system along with a plausible sensory motor feedback control unit based on the vestibular system that may be used to maintain the equilibrium position. In §3, we analyse the linearized dynamics of our model and derive an optimal feedback controller for posture control in the presence of limited information about

*Author for correspondence (lm@seas.harvard.edu).

Received 31 January 2012
Accepted 23 March 2012

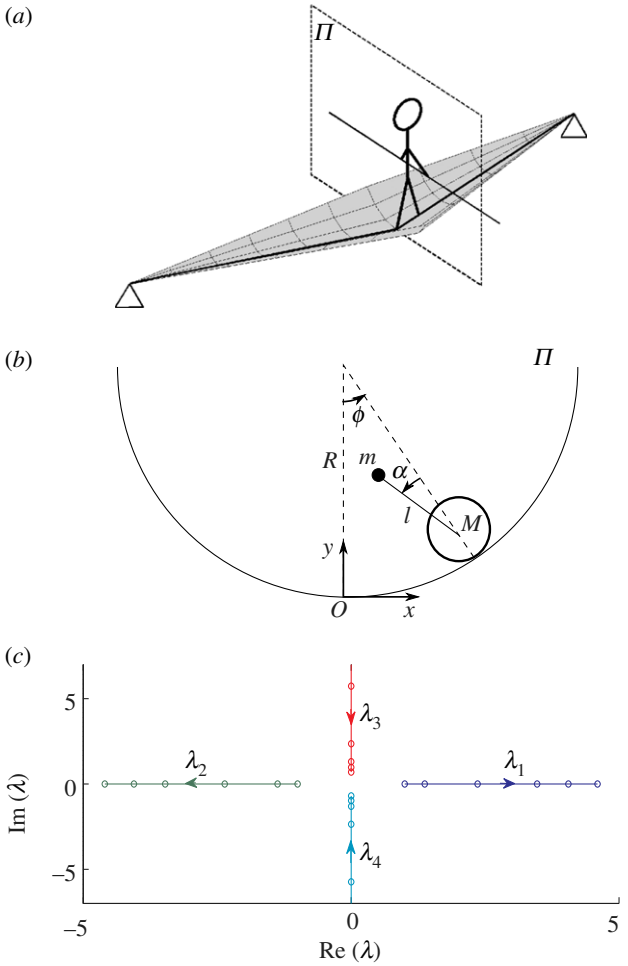

Figure 1. (*a*) Schematic of a man balancing on a rope and (*b*) associated mechanical model describing the transverse motion on the plane $\boldsymbol{\Pi}$. The linearized equations of motion for this system are reported in (3.1) and (3.2). (*c*) Spectrum of the linearized system defined in (3.1) and (3.2) as a function of R (top). The circular markers correspond to $R = 0, 0.5, 1, 1.5, 2, 3$. The markers for the imaginary eigenvalues for $R = 0$ is missing because $|\lambda_3| = |\lambda_4| \to \infty$ as $R \to 0$. (Online version in colour.)

the state space. The performance of this control law is tested in §4 on the full nonlinear model. Finally, in §5, we conclude with a discussion of the sensitivity of our model to additional effects such as the coupling between parameters, the effects of delay and outline some future directions of study.

2. MATHEMATICAL MODEL

2.1. Mechanics

A schematic of a man on a high wire is shown in figure 1. To develop a minimal model of the system that allows for analysis, we make several simplifying assumptions. Firstly, although the number of degrees of freedom of a human body is large, it is only the slow modes associated with the long limbs that are typically relevant since they are relatively easy to actuate for the purposes of balance. Here, we consider a model with only one degree of freedom associated with the orientation of the body, modelled as a simple inverted pendulum. Similarly, we model the rope as a (possibly) tensioned string that is deformed by the body, envisaging two extreme limits: large tension that is typical of tightropes, and small tension typical of slacklines. In both cases, we neglect the additional rope tension caused by the body sway motion since it is negligible relative to the static tension caused by either the pretension or the body weight [15]. Within this setting, the presence of the rope thus does no more than introduce a kinematic constraint on the motion of the cart, forcing this latter to move on a circular track associated with the swinging of the rope at constant extension, an excellent approximation for slacklines. The limit of very large pretension, i.e. small sag, however is not so trivial as there are three possible scenarios. In the simplest setting, but also probably the least realistic, we assume that the presence of the rope can be still assimilated via a kinematic constraint on the cart motion. This does not have to be true always—in particular, if one tries to recover the case of a pendulum on a fixed base, the ratio between the pendulum and cart inertia must vanish as $R \to 0$ to make sure the cart is not moving; this second situation is analysed in §5.1. Finally, elastic ropes with large pretension can still admit oscillations in orthogonal directions, but the horizontal and vertical motions become uncoupled. In this case, the rope introduces a dynamic, rather than a kinematic constraint on the motion of the cart and in §5.2, we introduce a third model for describing this situation.

Thus, our minimal dynamical system is an inverted pendulum (the body) placed on a cart (the rope) that moves on a circular track of radius R characterizing the envelope of transverse motions of the rope, shown in figure 1*b*. We note that R varies from zero near the rope supports to a maximum value when the man is at midspan, i.e. R is a parameter that identifies the position of the body along the rope. The inverted pendulum is assumed to have length l and a concentrated mass m on top, and its deviation from the radial direction is the angle α [8,16]. The cart is assumed to have mass M, with an angular position along the track given by the angle ϕ. We will initially consider R and $M + m$ as independent parameters by assuming, for example, that the rope pretension, and thus the sag, can be set at will, but will relax it eventually and in §5, we discuss the effects of a possible linear dependence between them induced by the elasticity of the rope.

The position of the cart (rope) relative to a fixed origin centred at O in figure 1*b* is $(x_M, y_M) = R\sin\phi$, $(R(1 - \cos\phi))$, while the position of the pendulum bob (body) is $(x_m, y_m) = (x_M - l\sin(\alpha + \phi), y_M + l\cos(\alpha + \phi))$, so that the Lagrangian of the system then reads

$$\begin{aligned} L = {} & \frac{1}{2}(M+m)R^2\dot{\phi}^2 - mRl\cos\alpha(\dot{\alpha}+\dot{\phi})\dot{\phi} + \\ & + \frac{1}{2}ml^2(\dot{\alpha}+\dot{\phi})^2 - (M+m)gR(1-\cos\phi) \\ & - mgl\cos(\alpha+\phi), \end{aligned} \tag{2.1}$$

where the first three terms represent the kinetic energy and the last two terms the gravitational potential energy.

Maintaining balance implies staying in a restricted region around the upright position corresponding to $\phi = 0$, $\alpha = 0$ so that we start with a focus on a linearized model of the dynamics (although we will later consider the complete dynamics). This linearized model around the unstable equilibrium with at most quadratic terms in the Lagrangian (2.1) then reads

$$\begin{aligned}\tilde{L} = &\frac{1}{2}(M+m)R^2\dot{\phi}^2 - mRl(\dot{\phi}^2 + \dot{\alpha}\dot{\phi}) + mRl\alpha^2 \\ &+ \frac{1}{2}ml^2(\dot{\alpha}+\dot{\phi})^2 - (M+m)gR\phi^2 \\ &- mgl[1-(\alpha+\phi)^2].\end{aligned} \tag{2.2}$$

The equations of motion for the system are then given by

$$\frac{\mathrm{d}}{\mathrm{d}t}\frac{\partial \tilde{L}}{\partial \dot{\mathbf{q}}} - \frac{\partial \tilde{L}}{\partial \mathbf{q}} = \mathbf{F}^q, \tag{2.3}$$

where $\mathbf{F}^q = (F^\phi, F^\alpha)$ represents the generalized force acting in the direction of the generalized coordinate q. Humans use their arms or a pole to maintain balance, this corresponds to a torque F^α on the inverted pendulum. Moreover, as the angle of the cart is not controlled, we have $F^\phi \equiv 0$. We have ignored the role of dissipation and damping in our model given its equivalence to the action of the torque F^α. It is convenient to express the dynamics in dimensionless form by defining $\bar{R} = R/l$, $\bar{m} = m/M$, $\bar{t} = \sqrt{g/l}t$, $\bar{F}^\alpha = F^\alpha/mgl$. Here, the scaled sag parameter $\bar{R}$ determines if one is in the tightrope or slackline limit, while the scaled body mass $\bar{m}$ is initially considered constant. Later, we assume that the cart mass is the sum of the mass of the feet (about 2% of the body mass [16]) and that of the rope; we initially set $\bar{m} \simeq 30$, but the overall behaviour of the system is relatively insensitive to the exact value of this parameter, as discussed in §5.1. For notational simplification, from now on we will always refer to dimensionless quantities without using the overbars.

2.2. Neurobiology

To complement the physical model with the neurobiological controller requires the specification of a suitable sensory cue that can be implemented via a physiological system and a concomitant control action implemented via an internal torque.

Complete knowledge of the full state of the system requires separate measurements of ϕ, $\dot{\phi}$, α and $\dot{\alpha}$, which is both unreasonable and unlikely. The three main sources of orientation measurements in humans are proprioceptive, visual and vestibular systems [13]. Precise information about absolute orientation with respect to the environment can be obtained by the visual system, but this introduces delays of the order of 100–200 ms [13], and are thus unlikely to be useful here given the fast timescales induced by the movable support, as we will see later. Proprioceptive sensors can measure the relative position and orientation between two joints of the body, but during balancing this information is inaccurate owing to the lack of a fixed reference for the cart (feet). However, fast and reliable measurements of body rotational and translational velocities are provided by the vestibular system located in the inner ear. The relative importance of these three sources varies accordingly to the motor task [13]. Experimental studies on quiet standing atop a sway-referenced platforms, i.e. the closest existing experimental set-up to our problem we are aware of, show that proprioceptive information quality is degraded and that the vestibular system starts to play a prominent role [2,7]. Since velocity measurements are more reliable than position and acceleration [17], we will assume that only the measurement of absolute angular velocity $\dot{\phi} + \dot{\alpha}$ is available for feedback control. This is motivated by the fact that vestibular system velocity estimate is the most accurate among available body sway measures and as we will prove, this limited information is enough to correctly estimate the full state of the system. This is also a very conservative model since it corresponds to the worst case scenario where we completely neglect visual, proprioceptive and absolute inclination measurements. However, it is worth noting that our results are robust to different choices of sensory input; for example, the same qualitative behaviour is observed if we assume that $\dot{\alpha}$ and $\dot{\phi}$ are measured separately by the proprioceptive system, or even in the ideal case when the whole state can be measured. For the control action, we assume that balancing around the upright position is achievable using the torque F^α [8] that is assumed to be bounded, i.e. $|F^\alpha(t)| \leq F^\alpha_{\max}$ (see appendix C for a simple derivation of an upper bound on the scaled torque ${F^\alpha}_{\max} \simeq 0.3$). Once again, our results are quite insensitive to the particular choice of $F_{\max}$; we can vary this quantity by a factor of 10 (for example, by considering potential torso and leg movements) without affecting the overall qualitative behaviour of the system.

For control strategies, we have a choice of continuous or discontinuous control strategies. The latter has been proposed for stabilization of quiet upright stance [18–21], based on the assumption that small deviations from upright position are not detected by the control unit and that active corrective torques are generated only when the position [19] or the velocity [20] exceeds a given threshold, i.e. when $|\alpha(t)| > \alpha_{\mathrm{cr}}$ or $|\dot{\alpha}| > \dot{\alpha}_{\mathrm{cr}}$. In the case under study, the coupling with the rope dynamics amplifies the sway dynamics and therefore the time spent inside the uncontrolled region $|\alpha(t)| \leq \alpha_{\mathrm{cr}}$, $|\dot{\alpha}(t)| \leq \dot{\alpha}_{\mathrm{cr}}$ is small, so that a continuous strategy might be practically equivalent to an intermittent control. Intermittent control strategies have also been proposed to cope with the intrinsic delay that is present in the feedback loop during quiet standing, exploiting the intrinsic stable manifold of the pendulum dynamics to passively drive the system towards the equilibrium [22]. Although such an approach can explain several experimental observations about quiet standing, its relevance for the problem at hand is not obvious. In fact, replacing the fixed base with a rope couples the dynamics of the rope to that of the human on it, so that the argument used for designing switching regions is invalid because the state space has now four-dimensional instead of two-dimensional.

Moreover, since the maximum admissible delay in our system is of the order of 40–70 ms (see §5.3), and thus shorter than the typical 100–200 ms, the performance gap between intermittent and continuous strategies is minimal, and therefore we focus here only on continuous feedback control.

3. ANALYSIS AND CONTROL

Before we discuss the controller, we first discuss the linearized dynamics of the system about the upright position.

3.1. Linearized dynamic analysis

The state of the system can be represented as $\mathbf{x} = (\phi, \dot{\phi}, \alpha, \dot{\alpha})$ with the input torque $u = F^{\alpha}$. Then the linearized non-dimensional dynamics (see appendix A for the full nonlinear dynamics) is given by

$$\dot{\mathbf{x}}(t) = \mathbf{A}\mathbf{x}(t) + \mathbf{B}u(t), \tag{3.1}$$

and

$$\left.\begin{aligned} \mathbf{A} &= \begin{bmatrix} 0 & 1 & 0 & 0 \\ -1/R & 0 & m/R & 0 \\ 0 & 0 & 0 & 1 \\ 1/R & 0 & 1+m-m/R & 0 \end{bmatrix} \\ \mathbf{B} &= \begin{bmatrix} 0 \\ m(R-1)R^2 \\ 0 \\ 1+m+m(1-2R)R^2 \end{bmatrix}. \end{aligned}\right\} \tag{3.2}$$

The linear stability of the upright position is completely characterized by the spectrum of the matrix $\mathbf{A}$ and is shown in figure 1*c* as a function of R (see also appendix B). We note that as R increases the magnitude of the real eigenvalues also increases, so that the system instability becomes severe, making control more difficult for large R. However, simultaneously, the imaginary eigenvalues move towards the origin, so that the natural frequencies of the system decrease and make control easier due to the absence of high frequencies in the system response. On the other hand, as R decreases, the system instability becomes less severe but the presence of high-frequency oscillations makes the model less likely to be accurate, because the dynamics of the rope can no longer be neglected and the control task becomes harder because the controller has to damp out such fast oscillations. The competition between these two effects suggests the existence of an optimum sag R, and thus a location along the tightrope/slackline where it is easiest to balance for a given mass ratio m.

In any case, for all R, the presence of one unstable mode requires the presence of a controller to stabilize the upright position. To ensure the existence of a feedback controller capable of such a task requires that the system is controllable, i.e. that there exists an input F^{α} capable of steering the system to the desired position. In a linear setting, this condition states that the system is controllable if and only if the controllability matrix $\Xi = [\mathbf{B}\,\mathbf{A}\mathbf{B}\ldots\mathbf{A}^{n-1}\mathbf{B}]$ has full rank [23]. In our model, Ξ is always full-rank so that a suitable linear controller always exists (appendix B). However, as $R \to 0$ or $R \to +\infty$ the matrix has a weak rank deficiency; in figure 2*b*, the condition number κ of the matrix Ξ is plotted as a function of R and shows that a minimum occurs at $R \simeq 1$.

As discussed in §2, partial measurements of the full state $(\phi, \dot{\phi}, \alpha, \dot{\alpha})$ are provided by $\dot{\phi} + \dot{\alpha}$ via the vestibular system. To check that the system is observable, i.e. that the reconstruction of the full state $\mathbf{x}$ from $\dot{\phi} + \dot{\alpha}$ is possible, we first write the measurement equation $y(t) = \dot{\phi}(t) + \dot{\alpha}(t)$ as

$$y(t) = \mathbf{C}\mathbf{x}(t) \tag{3.3}$$

with $\mathbf{C} = [0, 1, 0, 1]$. In the linear setting, observability reduces to testing that the associated observability matrix Ω has full rank [23], where

$$\Omega = \begin{bmatrix} \mathbf{C} \\ \mathbf{C}\mathbf{A} \\ \vdots \\ \mathbf{C}\mathbf{A}^{n-1} \end{bmatrix}. \tag{3.4}$$

In our model, Ω has full-rank for each value of R and M (appendix B), but as $R \to 0$ and $R \to +\infty$, Ω shows again a weak rank deficiency as reported in figure 2 that also shows that the minimum condition number occurs when $R \simeq 1$.

3.2. Optimal control strategy

Given the complete controllability and observability properties of our linearized model, it is also possible to stabilize the pendulum dynamics via a feedback controller, but the control strategy is not unique. Here, we focus on an optimal output feedback controller that takes the form of an LQG (linear quadratic Gaussian) controller, consisting of two parts: an optimal controller (linear quadratic or simply LQ regulator) given full state measurements and an optimal observer (Kalman filter) to estimate the full state given partial measurements, with the overall control scheme shown in figure 2 (see appendix C for a comparison of the case with complete measurements and that with limited information).

Since we want to minimize deviations from the upright position $\phi = \alpha = 0$, we choose a performance index

$$J(u) = \int_0^{+\infty} [q_{\phi}\phi^2 + q_{\alpha}\alpha^2 + F^{\alpha^2}]\mathrm{d}t, \tag{3.5}$$

where we have assumed an infinite time horizon for simplicity and we have set the weights $q_{\phi} = q_{\alpha} = 10$ in order to obtain stabilization for a wide range of R[1], while enlarging the basin of stabilization by limiting large variations in ϕ that would bring the system out of the range where linearization is valid. We do not weight the velocities $\dot{\phi}$ and $\dot{\alpha}$ so that we do not affect the controlled dynamics and deteriorate the performance. Recently, other authors [24] have analysed quiet standing using a two-link inverted

[1]The magnitude of these weights is quite different from Qu *et al.* [9] where the authors study the balancing problem on the sagittal plane with the feet on a fixed platform. However, what matters in LQ design is the relative magnitude among the various weights and in this perspective our choice is quite close to the one reported in the study of Qu *et al.* [9].

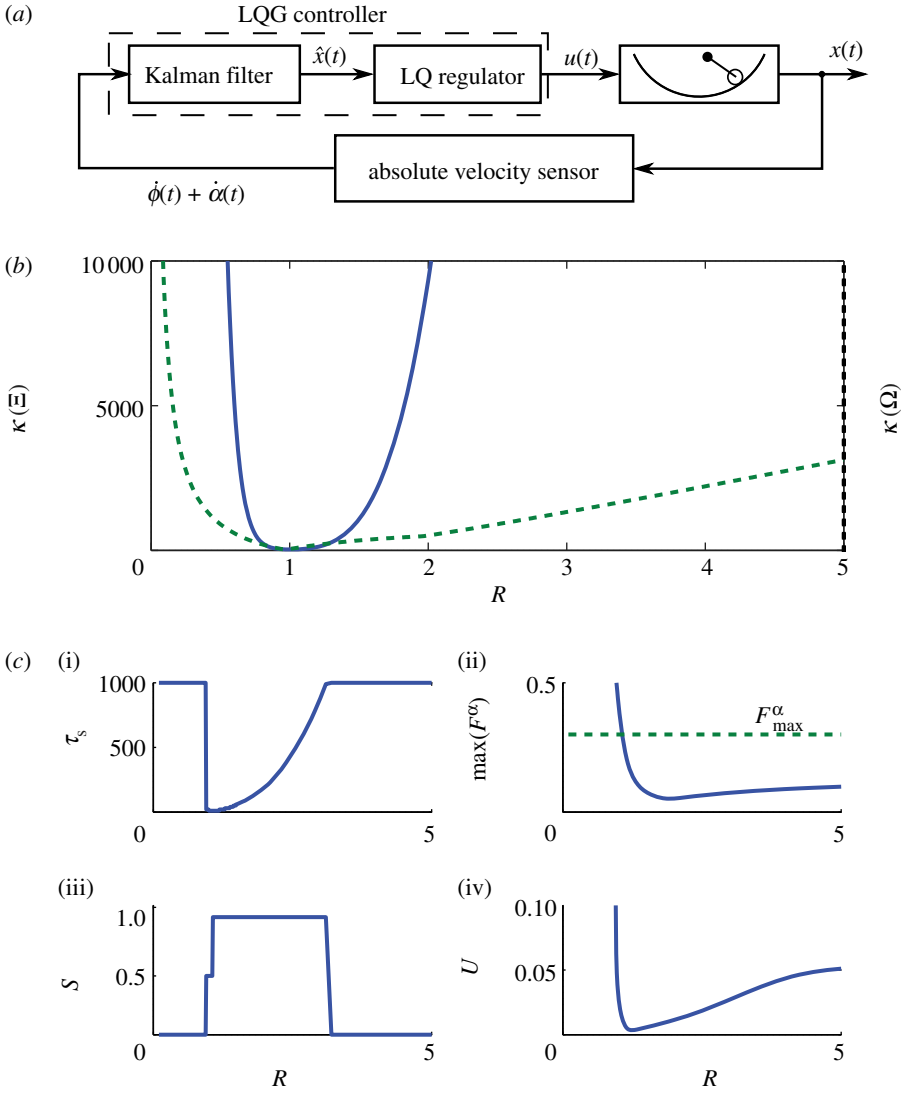

Figure 2. (*a*) Schematics of the balancing control loop. (*b*) Condition number κ of the controllability matrix Ξ (solid) and observability matrix Ω (dashed) as a function of normalized radius R. (*c*) Influence of the normalized radius R on time to steady state τ_s (i), maximum control torque $\max(F^{\alpha})$ (ii), stabilization S (iii) and energy spent for control U (iv). Data obtained by simulating the full nonlinear model (A 3) and (A 4) with $m = 30$ and LQG controller based on measurement of $\dot{\phi} + \dot{\alpha}$ (see §3.2). (Online version in colour.)

pendulum model to show that balance can also be achieved by minimizing a linear combination of angular deviations and velocities of the two links instead of using the classical centre-of-mass displacement minimization. We argue that the presence of a swaying rope makes our strategy similar to that proposed in the study of Kiemel *et al.* [24] because deviations from the vertical are automatically reflected in rope swaying motion and centre-of mass displacement. Defining three matrices $\mathbf{Q} = \mathrm{diag}(q_\phi, 0, q_\alpha, 0)$, $\mathbf{H} = 1$, $\mathbf{N} = 0$, the performance index (3.5) can be written as

$$J(u) = \int_0^{+\infty} [\mathbf{x}^{\mathrm{T}}\mathbf{Q}\mathbf{x} + u^{\mathrm{T}}\mathbf{H}u + \mathbf{x}^{\mathrm{T}}\mathbf{N}u]\mathrm{d}t. \tag{3.6}$$

Given the values of $\mathbf{Q}$, $\mathbf{H}$ and $\mathbf{N}$, the control input that minimizes the performance index $J(u)$ can be expressed as

$$u(t) = -\mathbf{K}\mathbf{x}(t), \tag{3.7}$$

where the optimal feedback gain $\mathbf{K}$ is determined by the unique symmetric positive definite solution $\mathbf{P}$ of an algebraic matrix Riccati equation [25]

$$\mathbf{K} = \mathbf{H}^{-1}(\mathbf{B}^{\mathrm{T}}\mathbf{P} + \mathbf{N}) \tag{3.8}$$

and

$$\mathbf{A}^{\mathrm{T}}\mathbf{P} + \mathbf{P}\mathbf{A} - (\mathbf{P}\mathbf{B} + \mathbf{N})\mathbf{H}^{-1}(\mathbf{P}\mathbf{B} + \mathbf{N})^{\mathrm{T}} + \mathbf{Q} = 0. \tag{3.9}$$

In order to compare the influence of the system parameters R and m on the controller performance, we fix the cost (3.6) and allow the feedback gain $\mathbf{K}$ to change according to (3.8) and (3.9).[2]

In the presence of noise in the sensor measurements and information processing, and because we only have partial information, the LQ regulator (3.7) is not sufficient and must be supplemented by an estimate $\hat{\mathbf{x}}$ of the true state

[2]The opposite strategy, i.e. the comparison of controller performance with fixed feedback gain $\mathbf{K}$ is not viable because the feedback gain designed for a given value of the parameters (and thus for a given $\mathbf{A}$ and $\mathbf{B}$) can be even non-stabilizing for different values of parameters.

variable $\mathbf{x}$, so that the optimal control input now reads

$$u(t) = -\mathbf{K}\hat{\mathbf{x}}(t). \tag{3.10}$$

To estimate $\hat{\mathbf{x}}$ given noisy and limited measurement $y(t) = \dot{\boldsymbol{\phi}}(t) + \dot{\boldsymbol{\alpha}}(t)$, while preserving the optimality of the control design, we design a Kalman filter as an optimal observer that gives a minimum-variance estimate of the system state variables. In the presence of noise on the internal dynamics and in the measurement process, (3.1) and (3.3) read

$$\dot{\mathbf{x}}(t) = \mathbf{A}\mathbf{x}(t) + \mathbf{B}u(t) + \mathbf{G}w(t) \tag{3.11}$$

and

$$y(t) = \mathbf{C}\mathbf{x}(t) + v(t). \tag{3.12}$$

where $w(t)$, $v(t)$ are stochastic variables, $\mathbf{G}$ is a gain vector linking the scalar noise $w(t)$ to the vectorial state variable $\dot{\mathbf{x}}(t)$, and the stochastic variables have zero mean and variance $\boldsymbol{\Sigma}$ and $\boldsymbol{\Theta}$, respectively. Then the Kalman filter dynamics can be written as

$$\dot{\hat{\mathbf{x}}}(t) = \mathbf{A}\hat{\mathbf{x}}(t) + \mathbf{B}u(t) + \mathbf{L}(y(t) - \hat{y}(t)) \tag{3.13}$$

and

$$\hat{y}(t) = \mathbf{C}\hat{\mathbf{x}}(t), \tag{3.14}$$

where the matrix gain $\mathbf{L}$ is derived from the positive definite solution $\mathbf{S}$ of an algebraic Riccati equation [25]

$$\mathbf{L} = \mathbf{S}\mathbf{C}^{\mathrm{T}}\boldsymbol{\Theta}^{-1} \tag{3.15}$$

and

$$\mathbf{A}\mathbf{S} + \mathbf{S}\mathbf{A}^{\mathrm{T}} + \mathbf{G}\boldsymbol{\Sigma}\mathbf{G}^{\mathrm{T}} - \mathbf{S}\mathbf{C}^{\mathrm{T}}\boldsymbol{\Theta}^{-1}\mathbf{C}\mathbf{S} = 0. \tag{3.16}$$

We note that the Kalman filter (3.12) and (3.13) can be viewed as a copy of the original system (3.1)–(3.3) with an additional input $y(t) - \mathbf{C}\hat{\mathbf{x}}(t)$ that allows for corrections to the estimates based on actual measurements.

In absence of noise, i.e. if $\boldsymbol{\Sigma} = \boldsymbol{\Theta} = 0$, equations (3.15) and (3.16) can be satisfied by taking $\mathbf{S} = 0$ and arbitrary $\mathbf{L}$. However, we use a 'virtual noise' to allow the system to be controlled in a weakly nonlinear regime. We choose $\boldsymbol{\Sigma} = \boldsymbol{\Theta} = 10^{-6}$ and $\mathbf{G} = [100,\ 100,\ 10,\ 10]^{\mathrm{T}}$ so that the noise amplitude on $\boldsymbol{\alpha}$ is in agreement with the result reported in the work of Boulet *et al.* [26] and the coefficients of variation of $\mathbf{G}w(t)$ with respect to $\boldsymbol{\alpha}(0)$ and $\boldsymbol{\phi}(0)$ read, respectively, 0.5 and 5. The noise in $\boldsymbol{\phi}$ is assumed to be larger than the noise in $\boldsymbol{\alpha}$ because deviations from $\boldsymbol{\phi} = 0$ quickly invalidate the linearized model and thus the controller design. Finally, we note that, although we do not have any experimental measurement of such noise parameters, the qualitative behaviour of the system is robust to changes in these parameter values, the more sensitive being the ratio between the noise on $\boldsymbol{\alpha}$ and the noise in $\boldsymbol{\phi}$, and all the results presented below still hold.

4. SIMULATIONS

To verify the performance of our linear control design, we now test it on the full nonlinear model. This is required as the same linearized model used for controller design could potentially hide performance degradation due to large deviations from the equilibrium position that dramatically changes the local response of the model to actuation. Such large deviations are indeed the main cause for instability in the closed loop system, as shown below, but they will be correctly compensated in the linearized model, although with large controller efforts. We simulate the system with initial conditions $\boldsymbol{\alpha}(0) = -1^{\circ}$, $\boldsymbol{\phi}(0) = 1^{\circ}$ and $\dot{\boldsymbol{\alpha}}(0) = \dot{\boldsymbol{\phi}}(0) = 0$ until $t_f = 1000$ which in dimensional terms corresponds to a few minutes.

To obtain a quantitative measure of the performance, we need to define one or more performance indexes. Two natural choices are the time τ_{s} needed to reach the steady state, defined as $\boldsymbol{\alpha}(\tau_{\mathrm{s}}) \leq 0.1\boldsymbol{\alpha}(0)$ and $\boldsymbol{\phi}(\tau_{\mathrm{s}}) \leq 0.1\boldsymbol{\phi}(0)$, and the maximum torque $\max(F^{\alpha})$ applied by the controller. To detect situations where stabilization is achieved by using a maximum torque $\max(F^{\alpha}) > F^{\alpha}_{\max}$, we define an index of success S as

$$S = \begin{cases} 1 & \max\{F^{\alpha}(t)\} \leq F^{\alpha}_{\max} \quad \text{and} \quad \tau_{\mathrm{s}} \leq t_f \\ 0.5 & \max\{F^{\alpha}(t)\} > F^{\alpha}_{\max} \quad \text{and} \quad \tau_{\mathrm{s}} \leq t_f \\ 0 & \tau_{\mathrm{s}} > t_f \quad \text{or system unstable,} \end{cases} \tag{4.1}$$

where $F^{\alpha}_{\max} \simeq 0.3$ is the upperbound on the torque estimated in appendix D. Finally, we calculate the total mechanical energy spent in the balancing task as

$$U(R, m) = \int_0^{1000} |F^{\alpha} \cdot \dot{\boldsymbol{\alpha}}| \mathrm{d}t, \tag{4.2}$$

where the absolute value of the mechanical power is used because muscles have to consume energy to perform negative work as well. The behaviour of these performance indices as functions of the sag R is summarized in figure 2*c*. We note that there is a range of R, centred around the equivalent body height, where all the performance indices show a global minimum. In this range, stabilization is achieved in a very short time $\tau_{\mathrm{s}} \simeq 3$ s, and the required torque is small $\max(F^{\alpha}) \simeq 30$ N, so that the required energy drops to a value as small as $U \simeq 3$ J. In the limit $R \to 0$, the balancing performances is severely degraded and the system can even become unstable. For large R, the system is actually stabilized by the controller, but the time needed for stabilization is larger than the total simulation time t_f and therefore the performance index $S \to 0$ as $R \geq 3.2$. We note that this behaviour is consistent with our linearized dynamic analysis in §3.1.

5. ADDITIONAL EFFECTS: PARAMETER COUPLING, DELAY AND DECOUPLED MOTIONS

So far, the two dimensionless variables in the model m and R have been assumed to be independent, and furthermore, we assumed that no delay was present. We now turn to address how balancing performance is affected by different choices for m, the potential dependence of the sag R on the mass m, as well as the singular limit $R \to 0$ where the horizontal and the vertical displacements of the rope become independent, and the presence of delay.

5.1. *Influence of mass-ratio* m *and normalized sag* R

In figure 3*a*,*b*, the behaviour of the total energy as a function of R and m is reported for two different

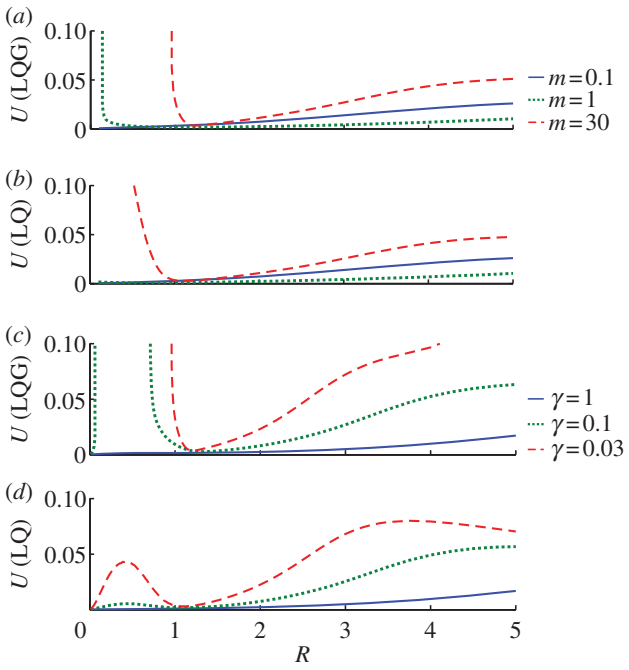

Figure 3. Total control energy spent for stabilization as a function of system parameters m and R. Data obtained by simulating the full nonlinear model (A 3) and (A 4) and (*a*) LQG controller based on measurement of $\dot{\phi}+\dot{\alpha}$ (solid line, $m=0.1$; dotted line, $m=1$; dashed line, $m=30$; see §3.2) and (*b*) LQ controller with full state information (appendix B). For comparison, we also plot the total control energy spent for stabilization as a function of parameters R and γ. Data obtained by simulating the full nonlinear model (A 3) and (A 4) with $R=\gamma m$ and (*c*) LQG controller based on measurement of $\dot{\phi}+\dot{\alpha}$ (solid line, $\gamma=1$; dotted line, $\gamma=0.1$; dashed line, $\gamma=0.03$; see §3.2) and (*d*) LQ controller with full state information (appendix C). (Online version in colour.)

controllers used for stabilization (refer to appendix C for the LQ case). We note that the energy has a global minimum whose position and magnitude are quite insensitive to the value of m. These results justify the use of a rough estimate for m, especially as the qualitative results are not strongly influenced by this choice. We note also that smaller values of m, typical for example of highwiring on steel ropes, allows for stabilization over a wider range of the rope sag R. In this situation, the control task becomes easier because applying a stabilizing torque on the pendulum does not induce large oscillations of the cart, and therefore, the nonlinearities responsible for the failure at small values of R are not excited by the control action. At the same time, for $R\gg 1$, the control torque cannot efficiently damp out the oscillations of the cart because it does not influence directly the cart dynamics, and therefore the time and thus the energy for stabilization increases, explaining why the energy for stabilization is not monotonic in m in the large sag limit.

We now turn to the case of an easily stretchable rope, such as a bungee cord, when R and m are no longer independent. Assuming minimally that $R=\gamma m$ with γ constant, implies that the body weight characterizes the radius of curvature of the rope. Then, we find that the results of the linearized dynamic analysis in §3.1 remain pertinent. In fact, we still get fast oscillations ($|\lambda_3|=|\lambda_4|\to+\infty$) as $R\to 0$ and fast unstable soft modes ($|\lambda_1|=|\lambda_2|\to+\infty$) for $R\to+\infty$. Similarly, the controllability and observability matrices show weak rank deficiency as $R\to+\infty$ and $R\to 0$, and therefore the required control effort increases in both limits. Thus, we still expect the presence of an optimal sag R where the controller achieves best balancing performance. We also note that within this model, we can correctly recover the limiting case of a pendulum on a fixed base since $m\to 0$ as $R\to 0$, i.e. the inertia of the cart becomes much bigger than the pendulum inertia.

In figure 3*c*,*d*, we plot the total control energy as a function of the radius R and the parameter γ. Decreasing γ, i.e. having larger m for a fixed radius R, forces the energy to increase as one can expect because it is easier balancing a light pendulum instead of an heavy one. We also note that as $R\to 0$ the control problem becomes trivial because we recover the limiting case of a pendulum on a fixed base and we control the angle α with a torque on α itself. The local maximum of the energy for small values of R arises form two competing factors: having small R and consequently small m makes the controller task easier, but at the same time the controllability and observability properties of the system become degenerate, and therefore, the controller cannot affect the dynamics efficiently. This is also the reason for the discrepancies between the LQ and LQG controllers behaviours for small R as the LQ controller does not suffer from the weak observability condition. It is worth noting that although fast oscillations are hard to observe and can be potentially damped out by viscous forces, the LQ controller still needs to compensate for them at the early stages of stabilization. However, owing to the reduced observability, the Kalman filter rate of convergence for $R\to 0$ becomes too slow and stabilization is precluded. Finally, for large R the degraded observability and controllability properties make the controller performance even worse than in the case of R independent by m, because the pendulum mass m increases as well and the system becomes more unstable.

5.2. *Alternative model when* $\mathbf{R}\ll 1$

The presence of the rope implies a kinematic constraint on the cart motion by forcing it to move on a circular track, and is equivalent to approximating the dynamics of the rope in terms of its softest mode. As the pretension in the rope becomes large and concomittantly the relative rope sag becomes small, the simple kinematic assumption loses its validity for two reasons: the mode is no longer soft and furthermore rope motion in the horizontal and vertical directions become uncoupled. Therefore, the model shown in figure 1*b* must be replaced by that in figure 4*a*. Here, the rope acts as a linear spring that tends to push the cart towards the rest position and the motion of the cart is limited primarily to a horizontal plane.[3]

[3]Here, we neglect the vertical displacement of the cart because in the linearized setting this quantity is neither controllable nor observable and therefore one has to rely only on the internal damping to stabilize this degree of freedom.

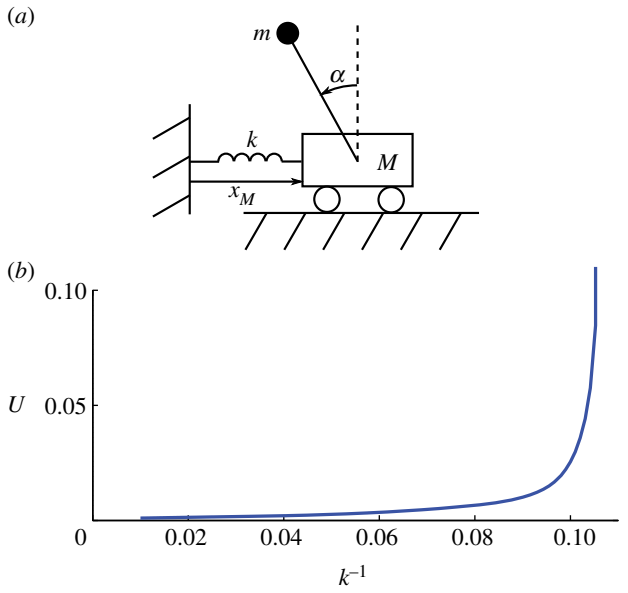

Figure 4. (*a*) Mechanical model for the motion on a tightrope with large pretension. The linearized equation of motion are reported in (5.2) and (5.3). (*b*) Total energy spent for stabilization as a function of spring stiffness k. Data obtained by simulating the full nonlinear model with LQG controller based on measurement of $\dot{\alpha}$. (Online version in colour.)

The equation of motion can be derived by considering as generalized coordinates $\mathbf{q}_T = (x_M, \alpha)^{\mathrm{T}}$, thus defining the Lagrangian

$$L_T = \frac{1}{2}(M+m)\,\dot{x}_M^2 + \frac{1}{2}m(l^2\dot{\alpha}^2 - 2l\dot{\alpha}x_M\cos\alpha) - \frac{1}{2}kx_M^2 - mgl\cos\alpha. \tag{5.1}$$

Following the same procedure in §§2.1 and 3.1, we can write the linearized dynamics in dimensionless form as

$$\dot{\mathbf{x}}_T = \mathbf{A}_T\mathbf{x}_T + \mathbf{B}_T u_T \tag{5.2}$$

and

$$\left.\begin{aligned}\mathbf{A}_T &= \begin{bmatrix} 0 & 1 & 0 & 0 \\ -k & 0 & m & 0 \\ 0 & 0 & 0 & 1 \\ -k & 0 & m+1 & 0 \end{bmatrix} \\ \mathbf{B}_T &= \begin{bmatrix} 0 \\ m \\ 0 \\ m+1 \end{bmatrix}\end{aligned}\right\} \tag{5.3}$$

where now $\mathbf{x}_T = (x_M, \dot{x}_M, \alpha, \dot{\alpha})^{\mathrm{T}}$ and k has been normalized by Mg/l. We note that as $R \to 0$ for the case when the cart is placed on a circular track the natural frequency of the system scales as $\sqrt{1/R}$, whereas in the current model the natural frequency scales as $\sqrt{k}$ so that large values of k correspond to small sag, as desired. Assuming as before that only the total angular velocity is measured, then

$$\mathbf{C}_T = [0 \quad 0 \quad 0 \quad 1]. \tag{5.4}$$

Finally, in order to obtain a fair comparison of the controller performance, we chose the same weights $\mathbf{Q}$, $\mathbf{H}$ and $\mathbf{N}$ for the LQ controller design and the same parameter values $\boldsymbol{\Sigma}$, $\boldsymbol{\Theta}$ and $\mathbf{G}$ of the Kalman filter as in §3.2.

In figure 4*b*, we report the total energy spent for stabilization as a function of the spring stiffness k. We note that the energy converges to a minimum as $k \to \infty$ that corresponds to balancing on a rigid support. As the stiffness decreases, the control becomes more difficult because the cart displacement tends to be larger and thus the system can be driven out of the range of validity of the linearized model.

5.3. *Influence of delay*

Measurement of the body orientation show a natural delay due to processing time of the information by the nervous system. Moreover, once the measurement is obtained, additional delays are introduced by the neural feedback controller that has to calculate the correct amount of torque necessary for stabilization and by the motor control system due to the neural signal travelling time and muscle activation delay. A delay in the feedback loop can severely reduce controller performance during balancing [8]. There is no agreement on the magnitude of the delay $\hat{\tau}$ mainly because human sensors/controller tend to adapt it accordingly to different tasks and different accurate measurements available [13]. Common estimates from experimental data range from 25 ms to 200 ms depending on the experimental conditions, with the delay decreasing proportionally to the utilization of the vestibular system [9,13,16] corresponding to values of scaled delay $\tau = \hat{\tau}\sqrt{g/l}$ between 0.07 and 0.63.

In the presence of delay in the control loop, the dynamics reads

$$\dot{\mathbf{x}}(t) = \mathbf{A}\mathbf{x}(t) + \mathbf{B}u(t-\tau), \tag{5.5}$$

i.e. it is represented by a delay differential equation, where we have lumped all the delays into a single term, using the linearity of our model to advantage. Since the magnitude of the delay is smaller than the typical timescale associated with the pendulum dynamics, i.e. $\tau < 1$, we approximate the delay variable $u(t-\tau)$ with its Taylor expansion up to the second order [9]

$$u(t-\tau) \simeq u(t) - \tau\dot{u}(t) + \frac{\tau^2}{2}\ddot{u}(t) \tag{5.6}$$

thus obtaining an extended system

$$\dot{\tilde{\mathbf{x}}}(t) = \tilde{\mathbf{A}}\tilde{\mathbf{x}}(t) + \tilde{\mathbf{B}}\tilde{\mathbf{u}}(t) \tag{5.7}$$

and

$$\tilde{y}(t) = \tilde{\mathbf{C}}\tilde{\mathbf{x}}(t), \tag{5.8}$$

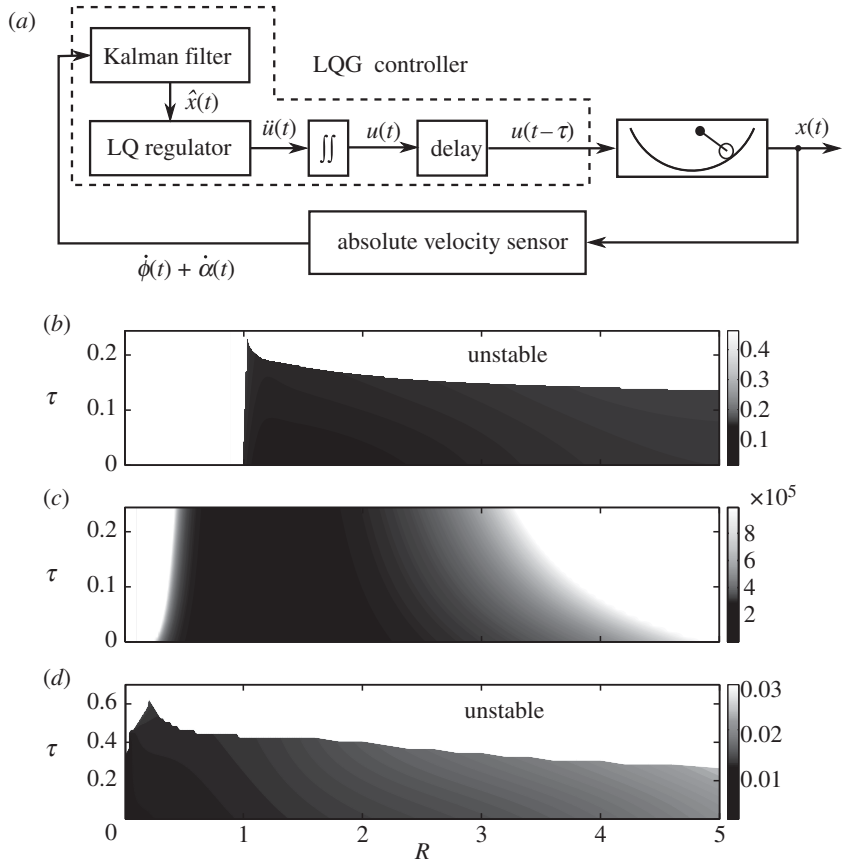

Figure 5. (*a*) LQG control system structure in presence of feedback delay τ. (*b*) Stability region and (*c*) controllability matrix condition number as a function of R and τ. Data obtained by simulating the full nonlinear model (A 3) and (A 4) with $m = 30$ and LQG controller based on measurement of $\dot{\phi} + \dot{\alpha}$. The white region corresponds to unstable dynamics, whereas the grey levels in the stability region code for the total amount of energy U spent for stabilizing the system. (*d*) Stability region as a function of R and $R = \gamma m$ with $\gamma = 1$ as in §5.1.

where

$$\tilde{\mathbf{x}} = \begin{bmatrix} \mathbf{x} \\ u \\ \dot{u} \end{bmatrix} \quad \text{and} \quad \tilde{u} = \ddot{u}, \tag{5.9}$$

and

$$\tilde{\mathbf{A}} = \begin{bmatrix} \mathbf{A} & \mathbf{B} & -\tau\mathbf{B} \\ \mathbf{0} & 0 & 1 \\ \mathbf{0} & 0 & 0 \end{bmatrix}, \quad \tilde{\mathbf{B}} \begin{bmatrix} \tau^2/2\mathbf{B} \\ 0 \\ 1 \end{bmatrix} \quad \text{and} \quad \tilde{\mathbf{C}} = [\mathbf{C} \quad 0 \quad 0]. \tag{5.10}$$

This allows us to design an LQG controller for the extended system that gives $\tilde{u}$ as a function of $\tilde{\mathbf{x}}$, and then we can integrate twice $\tilde{u}$ to obtain the input u for the original system, as illustrated by the block diagram in figure 5*a*.

However, observability analysis with $\tilde{\mathbf{A}}$ and $\tilde{\mathbf{C}}$ as in (5.10) shows that the system is no more completely observable, because the internal variables $(u, \dot{u})$ do not directly influence the output. However, we can easily overcome this problem by considering

$$\tilde{\mathbf{y}}(t) = \begin{bmatrix} \dot{\alpha}(t) + \dot{\phi}(t) \\ u(t) \\ \dot{u}(t) \end{bmatrix} \Rightarrow \tilde{\mathbf{C}} = \begin{bmatrix} \mathbf{C} & 0 & 0 \\ \mathbf{0} & 1 & 0 \\ \mathbf{0} & 0 & 1 \end{bmatrix}, \tag{5.11}$$

i.e. by adding measurements of the controller internal variable [9]. This assumption is not restrictive since the controller generates these signals by itself, thus it even does not need to measure them.

For the design of the extended system LQ regulator, we define a performance index as

$$\tilde{J}(u) = \int_0^{+\infty} [10\phi^2 + 10\alpha^2 + F^{\alpha^2} + \dot{F}^{\alpha^2} + 0.01\,\ddot{F}^{\alpha^2}]\mathrm{d}t, \tag{5.12}$$

where we choose to add a weight on $\dot{F}^{\alpha}$ to obtain better performance. In fact, when delay is present it can be convenient to slow down the dynamics of the controlled system so that the delay remains small compared with the typical closed loop timescale and the controller can easily compensate for it.

In figure 5*b*, we show the stability region as a function of the feedback delay τ and the normalized sag R. We note that increasing the value of the delay makes the performance worse and can lead the system to instability, as expected [8,27]. Since the natural frequency of the system decreases as $\sqrt{1/R}$ as $R \gg 1$, we expect the critical value of τ to increase as R becomes larger. The counterintuitive behaviour reported in figure 5*b* can be explained by noticing that the controllability matrix condition number

increases as τ increases as shown in figure 5*c*, thus this fact makes the control task actually harder. The same plot shows that for each value of τ the condition number reaches its minimum in a neighbourhood of $R=1$ and therefore the critical value of τ reaches its maximum in that region. Finally, in figure 5*d*, we show the region of stability as a function of the feedback delay when the sag R is proportional to the mass m as in §5.1. We note that in this case, the stable region becomes larger and, in particular, it encloses the origin because as $R\to 0$ and $\tau\to 0$ the problem reduces to the trivial stabilization of an inverted pendulum on a fixed base. However, for every value of the sag R there still exists a critical delay above which stabilization cannot be achieved.

5.4. Conclusions

A minimal mechanical model for the combined system of a human on a wire—an inverted pendulum mounted on a cart that is moving on a circular track—allows us to pose the problem of postural balancing on a tightrope or a slackline as an optimal control problem. We show that the measurement of the absolute angular position alone is enough to generate a feedback corrective torque that stabilizes the upright position. Our analysis also shows that there exists an optimal range of the rope sag where the balancing task is accomplished with minimal energy effort, in agreement with empirical experimental evidence [28].

More generally, tightrope walking and slacklining are just two examples of situations where the coupling of (active) internal body dynamics to (passive) external substrate dynamics both constrains and poses challenges for the neurophysiological performance of motor systems. Recent experimental studies have shown that postural sway analysis can be used to quantify changes in body or neural control due to pathologies [3], traumas [4] or ageing [29]. Complementing such data with mathematical models like the one we have proposed can help to devise tests with better discrimination while possibly uncovering the reason for performance degradation with age.

We thank M. Venkadesan for fruitful discussions.

APPENDIX A. FULL NONLINEAR MODEL

The Euler–Lagrange equations (2.3) for ϕ and α read, respectively,

$$\begin{aligned}&(ml^2 - mlR\cos\alpha)\ddot{\alpha} + 2mRl\sin\alpha\dot{\alpha}\dot{\phi}\\&\quad + ((M+m)R^2 - 2mlR\cos\alpha + ml^2)\ddot{\phi} + mRl\sin\alpha\,\dot{\alpha}^2\\&\quad - mgl\sin(\alpha+\phi) + MgR\sin\phi = F^{\phi}\end{aligned} \tag{A 1}$$

and

$$\begin{aligned}&ml^2\ddot{\alpha} + (ml^2 - mlR\cos\alpha)\ddot{\phi} - mlR\sin\alpha\,\dot{\phi}^2\\&\quad - mgl\sin(\alpha+\phi) = F^{\alpha}.\end{aligned} \tag{A 2}$$

By normalizing the variables as described in §2.1, we can write the full nonlinear equations of motions as

$$\begin{aligned}\ddot{\phi} = &-\frac{m\sin\alpha}{D}\dot{\alpha}^2 + \frac{m\sin\alpha(R\cos\alpha - 1)}{D}\dot{\phi}^2 - 2\frac{m\sin\alpha}{D}\dot{\alpha}\dot{\phi}\\&+ \frac{m\cos\alpha\sin(\alpha+\phi)}{D} - \frac{(1+m)\sin\phi}{D}\\&+ \frac{m(R\cos\alpha - 1)}{RD}F^{\alpha} + \frac{m}{RD}F^{\phi}\end{aligned} \tag{A 3}$$

and

$$\begin{aligned}\ddot{\alpha} = &\frac{m\sin\alpha(1 - R\cos\alpha)}{D}\dot{\alpha}^2\\&+ \frac{R^2\sin\alpha(1+m) + m\sin\alpha(1 - 2R\cos\alpha)}{D}\dot{\phi}^2\\&+ \frac{(1+m)[R\sin(\alpha+\phi) + \sin\phi - R\sin(\phi-\alpha)]}{2D}\\&+ \frac{\sin\phi - m\sin(2\alpha+\phi)}{2D} + \frac{2m\sin\alpha(1 - R\cos\alpha)}{D}\dot{\alpha}\dot{\phi}\\&+ \frac{R^2(1+m) + m(1 - 2R\cos\alpha)}{RD}F^{\alpha}\\&- \frac{m(1 - R\cos\alpha)}{DR}F^{\phi},\end{aligned} \tag{A 4}$$

where $D = R(1 + m - m\cos^2\alpha)$.

APPENDIX B. LINEAR SYSTEM ANALYSIS

The spectrum of the uncontrolled dynamics (3.1) reads

$$\lambda(\mathbf{A}) = \begin{bmatrix} 1\sqrt{2R}\sqrt{[\Lambda + \sqrt{\Lambda^2 + 4R(1+m)}]}\\ -1\sqrt{2R}\sqrt{[\Lambda + \sqrt{\Lambda^2 + 4R(1+m)}]}\\ 1\sqrt{2R}\sqrt{[\Lambda - \sqrt{\Lambda^2 + 4R(1+m)}]}\\ -1\sqrt{2R}\sqrt{[\Lambda - \sqrt{\Lambda^2 + 4R(1+m)}]}\end{bmatrix} \tag{B 1}$$

and

$$\Lambda = -1 + mR + R - m. \tag{B 2}$$

Note that for each value of R and M there are always one real positive eigenvalue, one real negative eigenvalue and two purely imaginary eigenvalues, consistently with the Hamiltonian (conservative) nature of the system.

Finally, the controllability matrix Ξ reads

$$\Xi = \begin{bmatrix} 0 & \chi_2 & 0 & -\frac{\chi_2}{R} + \frac{m}{R}\chi_1\\ \chi_2 & 0 & -\frac{\chi_2}{R} + \frac{m}{R}\chi_1 & 0\\ 0 & \chi_1 & 0 & \frac{\chi_2}{R} + (1 + R\chi_2)\chi_1\\ \chi_1 & 0 & \frac{\chi_2}{R} + (1 + R\chi_2)\chi_1 & 0\end{bmatrix} \tag{B 3}$$

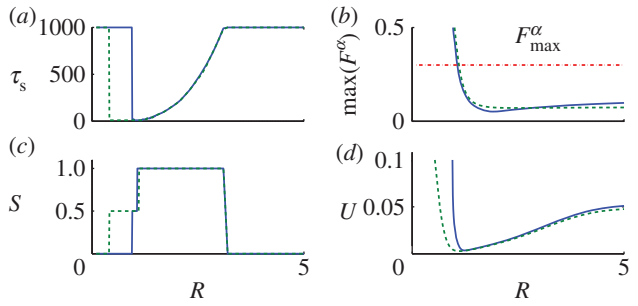

Figure 6. Influence of the normalized radius R on time to (*a*) steady-state τ_s, (*b*) maximum control torque $max(F^\alpha)$, (*c*) stabilization *success* and (*d*) energy spent for control U. Data obtained by simulating the full nonlinear model (A 3) and (A 4) with $m = 30$ and LQG controller (solid) or LQ controller (dashed). (Online version in colour.)

and

$$\chi_1 = \left(1 + m + m\frac{1-2R}{R^2}\right) \quad \text{and} \qquad \chi_2 = m\frac{R-1}{R^2}, \tag{B 4}$$

whereas the observability matrix $\boldsymbol{\Omega}$ can be written as

$$\boldsymbol{\Omega} = \begin{bmatrix} \mathbf{C} \\ \mathbf{CA} \\ \vdots \\ \mathbf{CA}^{n-1} \end{bmatrix} = \begin{bmatrix} 0 & 1 & 0 & 1 \\ 0 & 0 & \omega & 0 \\ 0 & 0 & 0 & \omega \\ \omega/R & 0 & \omega(\omega - m/R) & 0 \end{bmatrix} \tag{B 5}$$

and

$$\omega = 1 + m. \tag{B 6}$$

APPENDIX C. CONTROL WITH FULL STATE INFORMATION

In order to check that the behaviour observed in the §4 is not due to the lack of information about the true state of the system, we consider an ideal case where we have exact measurements of the all state variables, so that we can directly exploit the LQ regulator without any Kalman filter. The LQ design parameters are as in §4 so that we are not changing anything except the measurement equation (3.3) that becomes $\mathbf{y}(t) = \mathbf{x}(t)$, i.e. $\mathbf{C} = \mathbf{I}$.

In figure 6, a comparison between the two different control schemes is reported. We note that the lack of complete measurements on the full state does not massively degrade the system performances. The main difference is in the small radius limit, where a full information about the system variables allows the controller to stabilize the system with smaller values of R with respect to the LQG case, although with large corrective torque. Therefore, we can conclude that in the limit when $R \ll 1$, a strong source of instability is due to the poor state estimate provided by the Kalman filter. This result is in agreement to the observation that for small R the linearization validity basin is very narrow and high-frequency oscillations are present in the system, so that the linear observer can easily fail.

This analysis also shows that the difficulties that arise in the limits $R \to 0$ and $R \to +\infty$ are intrinsic in the system dynamics and are not due to the particular choice of control scheme, in agreement with the discussion of §3.1 about the controllability/observability properties and the validity of linear design.

APPENDIX D. TORQUE UPPERBOUND ESTIMATE

The main limitation in human balancing ability comes from the maximum value that the torque F^α can assume. We can estimate an upperbound for this quantity by considering the case in which the human uses a pole of mass m_p and length l_p supported by the two hands exerting forces F_1 and F_2 at a distance a from the pole centre of mass.

In order to support the weight $m_p g$ of the pole and generate a pure torque T, the forces F_1 and F_2 must satisfy $F_1 + F_2 = m_p g$, $F_1 a - F_2 a = T$. Then $T = (2F_{\max} - m_p g)a$. For the purpose of upperbound estimate, we can neglect the pole weight $m_p g$ with respect to the maximum force $F_{\max}$. Reasonable values for the parameters are $F_{\max} \simeq 250\,\mathrm{N}$ and $a \simeq 0.5\,\mathrm{m}$ so that $T_{\max} \simeq 250\,\mathrm{Nm}$ or, in dimensionless form, considering a body mass of about $m + M \simeq 80\,\mathrm{kg}$ and leg length $l \simeq 1\mathrm{m}$,

$$\bar{T} \simeq \frac{T}{mgl} = \frac{250}{80 \times 9.81 \times 1} \simeq 0.3. \tag{D 1}$$

The applied torque F^α is the negative of this quantity. Including potential torso and lateral leg movements in $F_{\max}$ would increase this value, but these movements are likely to be only emergency manoeuvres used only when the deviation from the upright position reaches extreme values. In any case, the qualitative behaviour of the system is quite insensitive to the exact value chosen for $F_{\max}$ and we can indeed increase it by an order of magnitude without severely affecting the observed behaviour, in accordance with the fact that the main difficulties for balancing on a rope are due to the structural property of the dynamics, such as controllability and observability, and not to the saturation on the control action. Here, we neglect potential 'wind-up' problems, i.e. situations when the arms or the pole start twirling, by assuming that the angular displacement of the pole from the horizontal position is always limited to a few degrees.

REFERENCES

1 Qu, X. & Nussbaum, M. A. 2009 Evaluation of the roles of passive and active control of balance using a balance control model. *J. Biomech.* **42**, 1850–1855. (doi:10.1016/j.jbiomech.2009.05.036)

2 Mahboobin, A., Loughlin, P. J., Redfern, M. S., Anderson, S. O., Atkeson, C. G. & Hodgins, J. K. 2008 Sensory adaptation in human balance control: lessons for biomimetic

robotic bipeds. *Neural Networks* **21**, 621–627. (doi:10.1016/j.neunet.2008.03.013)
3 Blaszczyk, J. W. & Orawiec, R. 2011 Assessment of postural control in patients with Parkinson's disease: sway ratio analysis. *Hum. Mov. Sci.* **30**, 396–404. (doi:10.1016/j.humov.2010.07.017)
4 Wikstrom, E. A., Fournier, K. A. & McKeon, P. O. 2010 Postural control differs between those with and without chronic ankle instability. *Gait Posture* **32**, 82–86. (doi:10.1016/j.gaitpost.2010.03.015)
5 Cabrera, J. L. & Milton, J. G. 2002 On–off intermittency in a human balancing task. *Phys. Rev. Lett.* **89**, 158702. (doi:10.1103/PhysRevLett.89.158702)
6 McDonald, J. H. G. 2009 Lateral excitation of bridges by balancing pedestrians. *Proc. R. Soc. A* **465**, 1055–1073. (doi:10.1098/rspa.2008.0367)
7 Peterka, R. J. & Loughlin, P. J. 2004 Dynamic regulation of sensorimotor integration in human postural control. *J. Neurophys.* **91**, 410–423. (doi:10.1152/jn.00516.2003)
8 Stepan, G. 2009 Delay effects in the human sensory system during balancing. *Phil. Trans. R. Soc. A* **367**, 1195–1212. (doi:10.1098/rsta.2008.0278)
9 Qu, X., Nussbaum, M. A. & Madigan, M. L. 2007 A balance control model of quiet upright stance based on an optimal control strategy. *J. Biomech.* **40**, 3590–3597. (doi:10.1016/j.jbiomech.2007.06.003)
10 Kiemel, T., Oie, K. S. & Jeka, J. J. 2002 Multisensory fusion and the stochastic structure of postural sway. *Biol. Cybern.* **87**, 262–277. (doi:10.1007/s00422-002-0333-2)
11 Otten, E. 1999 Balancing on a narrow ridge: biomechanics and control. *Phil. Trans. R. Soc. Lond. B* **354**, 869–875. (doi:10.1098/rstb.1999.0439)
12 Schweigart, G. & Mergner, T. 2008 Human stance control beyond steady state response and inverted pendulum simplification. *Exp. Brain Res.* **185**, 635–653. (doi:10.1007/s00221-007-1189-4)
13 Peterka, R. J. 2002 Sensorimotor integration in human postural control. *J. Neurophys.* **88**, 1097–1118. (doi:10.1152/jn.00605.2001)
14 Stepan, G. & Kóllar, L. 2000 Balancing with reflex delay. *Math. Comp. Model.* **31**, 199–205. (doi:10.1016/S0895-7177(00)00039-X)
15 Cheng, S. P. & Perkins, N. C. 1992 Free vibration of a sagged cable supporting a discrete mass. *J. Acoustical Soc. Am.* **91**, 2654–2662. (doi:10.1121/1.402973)
16 Cenciarini, M. & Peterka, R. J. 2006 Stimulus-dependent changes in the vestibular contribution to human postural control. *J. Neurophys.* **95**, 2733–2750. (doi:10.1152/jn.00856.2004)
17 Jeka, J., Kiemel, T., Creath, R., Horak, F. & Peterka, R. 2004 Controlling human upright posture: velocity information is more accurate than position or acceleration. *J. Neurophys.* **92**, 2368–2379. (doi:10.1152/jn.00983.2003)
18 Collins, J. J. & De Luca, C. J. 1994 Random walking during quiet standing. *Phys. Rev. Lett.* **73**, 764–767. (doi:10.1103/PhysRevLett.73.764)
19 Milton, J., Townsend, J. L., King, M. A. & Ohira, T. 2009 Balancing with positive feedback: the case for discontinuous control. *Phil. Trans. R. Soc. A* **367**, 1181–1193. (doi:10.1098/rsta.2008.0257)
20 Deligniéres, D., Torre, K. & Bernard, P.-L. 2011 Transition from persistent to anti-persistent correlations in postural sway indicates velocity-based control. *PLoS Comput. Biol.* **7**, e1001089. (doi:10.1371/journal.pcbi.1001089)
21 Kowalczyk, P., Glendinning, P., Brown, M., Medrano-Cerda, G., Dallali, H. & Shapiro, J. 2011 Modelling human balance using switched systems with linear feedback control. *J. R. Soc. Interface* **9**, 234–245. (doi:10.1098/rsif.2011.0212)
22 Asai, Y., Tasaka, Y., Nomura, K., Nomura, T., Casadio, M. & Morasso, P. 2009 A model of postural control in quiet standing: robust compensation of delay-induced instability using intermittent activation of feedback control. *PLoS ONE* **4**, e6169. (doi:10.1371/journal.pone.0006169)
23 Chen, C. 1999 *Linear system theory and design*, 3rd edn. New York, NY: Oxford University Press.
24 Kiemel, T., Zhang, Y. & Jeka, J. J. 2011 Identification of neural feedback for upright stance in humans: stabilization rather than sway minimization. *J. Neurosci.* **31** 15 144–15 153. (doi:10.1523/JNEUROSCI.1013-11.2011)
25 Goodwin, G. C., Graebe, S. F. & Salgado, M. E. 2001 *Control system design*. Upper Saddle River, NJ: Prentice Hall.
26 Boulet, J., Balasubramaniam, R., Daffertshofer, A. & Longtin, A. 2010 Stochastic two-delay differential model of delayed visual feedback effects on postural dynamics. *Phil. Trans. R. Soc. A* **368**, 423–438. (doi:10.1098/rsta.2009.0214)
27 Milton, J., Cabrera, J. L., Ohira, T., Tajima, S., Tonosaki, Y., Eurich, C. W. & Campbell, S. A. 2009 The time-delayed inverted pendulum: implications for human balance control. *Chaos* **19**, 026110. (doi:10.1063/1.3141429)
28 Balcom, S. 2005 *Walk the line: the art of balance and the craft of slackline*. Ashland, Oregon: SlackDaddy Press.
29 Du Pasquier, R. A., Blanc, Y., Sinnreich, M., Landis, T., Burkhard, P. & Vingerhoets, F. J. G. 2003 The effect of aging on postural stability: a cross sectional and longitudinal study. *Clin. Neurophysiol.* **33**, 213–218. (doi:10.1016/j.neucli.2003.09.001)